

# Adaptive two-regime method: application to front propagation

Martin Robinson,<sup>1, a)</sup> Mark Flegg,<sup>1, b)</sup> and Radek Erban<sup>1, c)</sup>

*Mathematical Institute, University of Oxford, Andrew Wiles Building, Radcliffe Observatory Quarter,  
Woodstock Road, Oxford OX2 6GG, United Kingdom*

(Dated: 16 August 2021)

The Adaptive Two-Regime Method (ATRM) is developed for hybrid (multiscale) stochastic simulation of reaction-diffusion problems. It efficiently couples detailed Brownian dynamics simulations with coarser lattice-based models. The ATRM is a generalization of the previously developed Two-Regime Method [Flegg et al, *Journal of the Royal Society Interface*, 2012] to multiscale problems which require a dynamic selection of regions where detailed Brownian dynamics simulation is used. Typical applications include a front propagation or spatio-temporal oscillations. In this paper, the ATRM is used for an in-depth study of front propagation in a stochastic reaction-diffusion system which has its mean-field model given in terms of the Fisher equation [Fisher, *Annals of Eugenics*, 1937]. It exhibits a travelling reaction front which is sensitive to stochastic fluctuations at the leading edge of the wavefront. Previous studies into stochastic effects on the Fisher wave propagation speed have focused on lattice-based models, but there has been limited progress using off-lattice (Brownian dynamics) models, which suffer due to their high computational cost, particularly at the high molecular numbers that are necessary to approach the Fisher mean-field model. By modelling only the wavefront itself with the off-lattice model, it is shown that the ATRM leads to the same Fisher wave results as purely off-lattice models, but at a fraction of the computational cost. The error analysis of the ATRM is also presented for a morphogen gradient model.

## I. INTRODUCTION

Deterministic mean-field models of reaction-diffusion systems describe the state of each chemical species using continuous variables (concentrations) and simulate its variation with time and space using reaction-diffusion partial differential equations (PDEs). Due to the wealth of analytical techniques available, such mean-field models have enjoyed considerable success<sup>1</sup>. However, there has been increasing interest in modelling the stochastic effects that arise from either a finite population size or the discrete nature of its individuals<sup>2,3</sup>. Stochastic models are often derived using a bottom-up approach, where the model is formulated using the individuals of the population as the basic entities, and the model parameters are chosen so that in the limit of large population size the model approaches known mean-field diffusion and reaction rates<sup>4-6</sup>. This type of model is sometimes termed an individual-based model (IBM)<sup>2</sup>.

Generally, different IBMs can be divided into one of two separate categories: off-lattice or lattice-based models. Off-lattice models treat each individual as a point in a continuous spatial domain. Different individuals are more likely to interact if they are located in a similar spatial location, i.e. the likelihood of interaction often depends on the distance between each pair<sup>7</sup>. Here we restrict our consideration to the diffusion and reaction of molecular species and use the term molecular-based instead of off-lattice model. Molecular-based simulations in this paper are formulated in the form of Brownian

dynamics<sup>5,8</sup>. Each molecule of each species is given a position in the spatial domain, and bimolecular reactions can occur whenever two molecules are separated by a given binding radius<sup>9</sup>.

Lattice-based models involve the discretization of the computational domain into a set of compartments (i.e. a lattice), upon which individuals can move by “jumping” between neighbouring compartments (i.e. connected lattice sites)<sup>10</sup>. In the applications which we shall consider, the individuals (molecules) do not have memory, that is, they do not remember which lattice site they came from. Therefore, compartment-based models are particularly suitable for efficient simulations, as only the number of molecules in each compartment is recorded. For this type of model the concept of a lattice has been replaced with a set of connected compartments, each with a specific volume. This volume, and the molecules within it, are assumed to be well-mixed. Reactions can only occur between molecules in the same compartment, and diffusion occurs by random jumps between neighbouring compartments<sup>7,10</sup>.

Different IBMs can exhibit different stochastic effects, even for large molecule numbers<sup>2</sup>. In particular, a well known reaction-diffusion system that exhibits a slow convergence to the mean field description is the Fisher travelling wave, the prototype model for the spread of a biological species<sup>11</sup>. For finite molecule numbers, stochastic effects can play a significant role in reducing the speed of the wave<sup>12</sup>, but the degree to which the wave speed is reduced depends on the details of the particular IBM used. Figure 1 shows snapshots from Fisher wave simulations using both compartment-based (top plot) and a molecular-based (middle plot) IBMs. The parameters and initial conditions are the same for both simulations and are discussed in Section III B. It is evident

<sup>a)</sup>Electronic mail: martin.robinson@maths.ox.ac.uk.

<sup>b)</sup>Electronic mail: mark.flegg@maths.ox.ac.uk.

<sup>c)</sup>Electronic mail: erban@maths.ox.ac.uk.

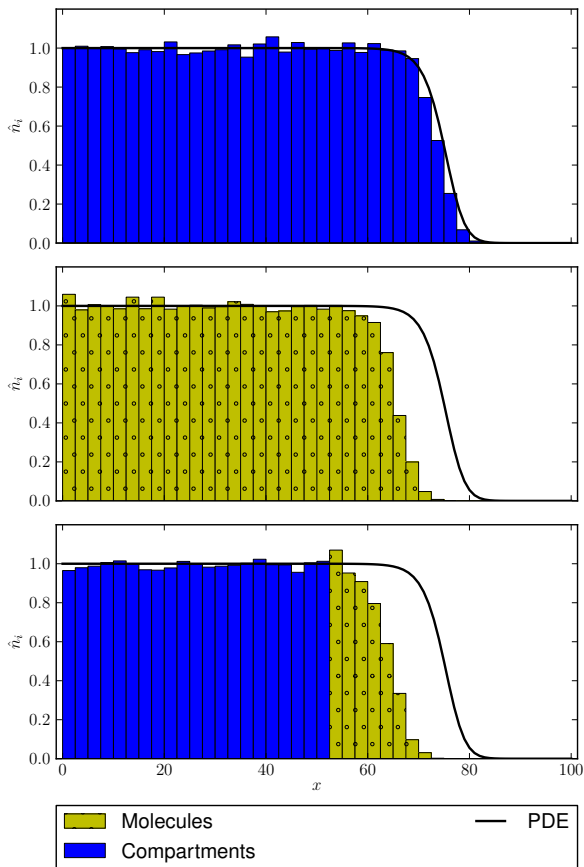


FIG. 1. Time snapshots of the profile of the stochastic Fisher wave (see Section III B for details) using different IBMs, demonstrating the differences in wave speed between the models. Top: Compartment-based simulation (Section II B); Middle: Molecular-based simulation (Section II A); Bottom: Coupled molecular-based and compartment-based simulation (Section II C). Plots show a histogram of scaled molecular concentration versus the  $x$ -coordinate. Boxes colored blue are compartment-based regions while yellow (with little circles) denotes a molecular-based region. The blue line shows a (deterministic) finite difference solution of the mean-field PDE (11).

that one obtains substantially different wave speeds depending on the IBM used, even though they would be both described by the same mean-field model. The solution of mean-field PDE (11) is shown as a solid blue line. Note that the mean-field model does not include any stochastic effects and thus should not be compared with the stochastic models in terms of solution accuracy. While the compartment-based IBM shown here is much closer to the mean-field model than the molecular-based IBM, this is merely an effect of the parameters used, and the results in Section III B show that the compartment-based wave speed is strongly dependent on the compartment size.

While there have been numerous investigations into

the speed of Fisher travelling waves for lattice or compartment-based IBMs<sup>12–15</sup>, molecular-based models have received little attention due to their heavy computational requirements, which scale up quickly as the total number of molecules increases. An alternative and more efficient approach is to simulate only the wavefront itself with a molecular-based IBM, while a less computationally intensive IBM is used in the remainder of the computational domain, particularly in the high concentration region behind the wavefront. This ensures that the dynamics of the wave are determined solely by the molecular-based IBM while keeping the total number of discrete molecules (and the computational requirements) to a minimum. An example of this (taken from the results shown in Section III B) is shown in Figure 1 (bottom), which matches the wave speed of the purely molecular-based simulation.

A related hybrid approach to stochastic Fisher wave simulation was taken by Moro<sup>16</sup>, who used a lattice-based model for the leading edge of the wavefront and a numerical approximation of the mean-field equation for the remainder of the domain. Moro’s aim was also to use a hybrid approach for computational efficiency, but was primarily interested in the lattice-based model for the Fisher wave. In contrast, our goal is to study the effects of using a molecular-based model of the Fisher wave, and we therefore use this method to simulate the wavefront.

In this paper, we develop the Adaptive Two-regime Method (ATRM) which is suitable for the efficient modelling of reaction-diffusion systems using both molecular-based and compartment-based IBMs. This is achieved by the coupling of the two different stochastic models across an interface separating two respective non-overlapping spatial regions. The ATRM is the generalization of the previously developed Two-Regime Method (TRM)<sup>17,18</sup> which allows a model to use different IBMs in regions in which they are required. One of the limitations of the TRM is that it has used a fixed domain decomposition. The ATRM generalizes TRM to any problem where the interface between the two regions can move over time, and therefore adapt to a dynamical chemical system (for example, travelling waves, regional population growth) or changes in the problem geometry (for example, cellular morphology). A simplified version of ATRM was used previously to simulate the growth of filopodia<sup>19</sup>, but the focus was on the application itself rather than the error introduced by the moving interface. The goal of this paper is to both fully characterise the moving interface error for three-dimensional reaction-diffusion simulations, and to demonstrate that it can reproduce the results of a much more computationally demanding molecular-based method when applied to a Fisher wave simulation.

The paper is divided into three main sections. In Section II, the different methods used in this paper are described. In Section III A, we investigate the error introduced by the moving interface and how it varies with the model parameters by applying the method to a steady-state morphological gradient problem. These results are

compared to both a static interface and purely molecular-based and purely compartment-based IBMs. Section IIIB describes the application of the ATRM to a Fisher wave. The speed of the modelled wave (corresponding to the interface speed) and the effect of the total number of molecules and the compartment size are investigated and compared with the purely molecular and compartment-based IBMs. We conclude our paper with discussion of our results and other hybrid (multiscale) methods for reaction-diffusion processes in Section IV.

## II. METHODS

The most detailed modelling approach considered in this paper will be given in terms of Brownian dynamics and introduced in Section IIA. We will use this model to study a Fisher wave in Section IIIB. The rest of the models introduced below will be used to decrease the computational intensity of the molecular-based model, while keeping the same level of accuracy.

### A. Molecular-based Modelling

We will study a time-driven molecular-based algorithm in this paper<sup>4</sup>. Time-driven molecular-based algorithms consider each molecule as a single point particle with position  $\mathbf{x}(t)$ . The molecular-based method proceeds with discrete timesteps  $\Delta t$ , and the diffusion of the molecules/particles is modelled as a discretized Brownian motion

$$\mathbf{x}(t + \Delta t) = \mathbf{x}(t) + \sqrt{2D\Delta t} \zeta, \quad (1)$$

where  $D$  is the diffusion constant and  $\zeta = [\zeta_x, \zeta_y, \zeta_z]$  is a vector of random numbers sampled from a normal distribution with zero mean and unit variance. Examples of software packages implementing a time-driven molecular-based method include Smoldyn<sup>4,20</sup> and MCell<sup>21,22</sup>.

The simulation of zeroth-order reactions (production from a source with a fixed rate) and first-order (unimolecular) reactions is relatively straightforward and makes use of a generator of Poisson and exponentially distributed random numbers<sup>4,10</sup>. Bimolecular reactions can occur whenever two reactant molecules come within a specified distance of each other. In the Fisher wave simulation in Section IIIB, we have the following reversible bimolecular reaction



with forward and backwards reaction rate constants  $k_2$  and  $k_1$ , respectively. To model it, we follow a generalization to the classical Smoluchowski model, where the forward reaction occurs within the binding radius  $\rho$  with probability  $P_{\Delta t}$  per timestep<sup>7</sup>. We also introduce an unbinding radius  $\alpha\rho$ , which is the distance that the two

molecules of  $A$  are placed apart, whenever the backward reaction in (2) occurs<sup>4</sup>. To calculate  $P_{\Delta t}$  and  $\alpha$ , we introduce the following dimensionless parameters

$$\gamma = \frac{\sqrt{4D\Delta t}}{\rho}, \quad \kappa = \frac{k_2\Delta t}{\rho^3},$$

where  $D$  is the diffusion constant of  $A$ . The reaction probability per timestep  $P_{\Delta t}$  can be found by solving (via a look-up table or root finding method)<sup>5</sup>

$$\kappa = 2\pi P_{\Delta t} \int_0^1 \xi^2 g(\xi; P_{\Delta t}, \gamma) d\xi, \quad (3)$$

where  $g(\xi; P_{\Delta t}, \gamma)$  is found by discretizing and solving numerically

$$\begin{aligned} g(r) = & (1 - P_{\Delta t}) \int_0^1 K(r, r'; \gamma) g(r') dr' \\ & + \int_1^\infty K(r, r'; \gamma) g(r') dr' \\ & + \frac{P_{\Delta t} K(r, \alpha; \gamma)}{\alpha^2} \int_0^1 g(r') r'^2 dr'. \end{aligned}$$

where

$$K(\xi, \xi'; \gamma) = (4\pi\gamma P_{\Delta t})^{-1/2} \exp\left(\frac{-(\xi - \xi')^2}{4\gamma P_{\Delta t}}\right)$$

is Green's function for the diffusion PDE.

### B. Compartment-based Modelling

The domain is partitioned into  $K$  compartments  $j = 0, 1, \dots, K$ . Whilst there has been significant progress in the field of irregular lattice compartment-based reaction-diffusion simulation<sup>6,23</sup>, here we restrict the partitioning to a regular grid of cube compartments with side length  $h$ . The molecules within each compartment are assumed to be well-mixed and are therefore evenly distributed over its volume. Without the need for position information, this method only stores the total number of each species contained within each compartment. In this paper, all models will only include one chemical species,  $A$ . We will denote the number of molecules of  $A$  in the  $j$ -th compartment as  $A_j$ .

The compartment-based algorithm is event-based. In this paper, we use a variant of the Next Subvolume Method<sup>24</sup> which is itself an extension of the Gillespie algorithm<sup>25</sup> and the Gibson-Bruck algorithm<sup>26</sup>. At the beginning of the simulation, the next event time  $t_j$  is generated for each compartment by

$$t_j = \frac{1}{\alpha_j} \ln\left(\frac{1}{u_0}\right), \quad (4)$$

where  $u_0$  is a uniformly distributed random number in  $(0, 1)$  and  $\alpha_j$  is the sum of propensities of all events

(reactions or diffusion jumps) which can occur in the  $j$ -th compartment. In the Fisher wave simulation in Section IIIB, we have two reactions in each compartment, given as the forward and backward reactions in (2). Diffusion events (instantaneous jumps from a compartment to an adjacent compartment) are considered as reaction events<sup>10</sup>, with a propensity  $D/h^2 A_j$ . Thus  $\alpha_j = k_1 A_j + k_2 A_j (A_j - 1) + 6D/h^2 A_j$  in (4) for the internal compartments, i.e. the compartments which have six neighbouring compartments. Boundary compartments have appropriately modified propensity functions because they have less neighbouring compartments<sup>27</sup>. Then the compartments are sorted by  $t_j$  using an index priority queue. At each step of the algorithm the compartment  $j_1$  with the smallest next reaction time is taken from the queue and an event is chosen using another uniformly distributed random number<sup>25</sup>. This event is processed and a new  $t_{j_1}$  is sampled for that compartment using

$$t_{j_1} = t + \frac{1}{\alpha_j} \ln \left( \frac{1}{u_0} \right),$$

where  $t$  is the current time. If the processed event is a diffusion jump to compartment  $j_2$ , then  $A_{j_2}$  also changes and the corresponding  $\alpha_{j_2}$  needs to be recalculated. Denoting its old value as  $\alpha_{j_2}^{old}$ , the old next event time  $t_{j_2}^{old}$  is updated using<sup>26</sup>

$$t_{j_2} = t + \frac{\alpha_{j_2}^{old}}{\alpha_{j_2}} (t_{j_2}^{old} - t). \quad (5)$$

Examples of software packages that implement the compartment-based model are MesoRD<sup>28</sup> and URDME<sup>23</sup>.

### C. Two-Regime Method

The Two-Regime Method (TRM) was originally presented in one spatial dimension<sup>17</sup> and later extended to higher-dimensional domains<sup>18</sup>. It considers the diffusion of molecules across the interface  $I$  between non-overlapping domains  $\Omega_C$  and  $\Omega_M$  modelled using compartment-based ( $\Omega_C$ ) and molecular-based methods ( $\Omega_M$ ), respectively.

The TRM optimally preserves the correct diffusion flux across the interface  $I$  between the regimes. To achieve this, a number of different factors must be taken into account. When particles cross the interface into the compartment domain  $\Omega_C$  they are placed in a compartment. Whilst these molecules would ordinarily be close to the interfacial side of the compartments in which they are placed, by virtue of being described using a compartment-based approach, they must be considered indistinguishable from other molecules “spread out” over the compartment volume. In order to counterbalance the generated net flux from the molecular-based domain  $\Omega_M$  into the compartment-based regime  $\Omega_C$  as a result of this

paradigm-critical loss of information, the propensity of a diffusion jump back across the interface  $I$  is specified differently to the other diffusive jump propensities using<sup>17</sup>

$$\frac{2h}{\sqrt{\pi D \Delta t}} \frac{D}{h^2} A_j,$$

where  $A_j$  is the number of molecules in the compartment next to the interface  $I$ . When a diffusion jump from  $\Omega_C$  across the interface (to the molecular-based side  $\Omega_M$ ) occurs the molecule is given a position in  $\Omega_M$  with a normal distance from the interface given by  $x$ , where  $x$  is sampled from<sup>17</sup>

$$f(x) = \sqrt{\frac{\pi}{4D\Delta t}} \operatorname{erfc} \left( \frac{x}{\sqrt{4D\Delta t}} \right). \quad (6)$$

The perpendicular distance  $x$  given by the distribution (6) is taken from an initial position on the interface given by  $\mathbf{r}_j$

$$\mathbf{r}_j = \mathbf{m}_j + y\mathbf{p}_1 + z\mathbf{p}_2,$$

where  $\mathbf{m}_j$  is the mid-point of the compartment face from which the diffusion jump occurred,  $\mathbf{p}_1$  and  $\mathbf{p}_2$  are perpendicular unit vectors tangential to the interface and aligned with the lattice vectors of the compartment-based domain. Random numbers  $y$  and  $z$  are sampled from the triangular distribution with lower limit  $-h/2$ , upper limit  $h/2$  and zero mean<sup>18</sup>.

The TRM has been used previously to study filopodia dynamics<sup>19</sup> and intracellular calcium release from ion channels<sup>29</sup> whereby a small-scale biochemical system is coupled with a coarser model in a much larger domain.

### D. Adaptive Two-Regime Method

In this paper we introduce the Adaptive Two-Regime Method (ATRM), a method for changing the compartment and molecular-based subdomains  $\Omega_C$  and  $\Omega_M$  in response to the outcome and requirements of a dynamic reaction-diffusion simulation. This is achieved by moving the interface  $I \equiv I(t)$  between simulation regimes. Whilst the methodology introduced in this paper can be generalized for any criteria defining the dynamic interface, we move the interface  $I(t)$  in such a way as to limit the computational requirements of the molecular-based subdomain  $\Omega_M$  (which can otherwise become too cumbersome). We will not be considering time-adapting lattices in the compartment-based model and therefore the moving interface  $I(t)$  moves discretely such that the interface aligns with the faces of the compartments. The compartment geometry that we consider in this paper is a regular grid of equal sized cubes with side length  $h$  (see Figure 2). The interface  $I(t)$  is constrained to move by step sizes equal to  $h$  in a direction normal to the interface surface, so that it is always flat and aligned to the faces of those compartments on the boundary.

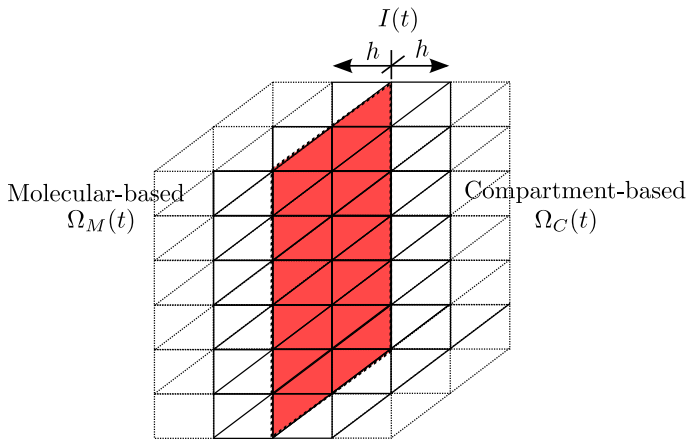


FIG. 2. The interface  $I(t)$  between the molecular and compartment regions (red surface) is restricted to move by jumps between neighbouring compartment faces.

The conditions on the movement of the interface can be set according to the specific problem. However, an obvious and useful goal is that the interface  $I(t)$  moves to restrict the total number of particles in  $\Omega_M$ , therefore placing a limit on the computational effort applied to the method that is expected to be the most computationally demanding.

Following this goal, we move the interface towards the molecular-based region  $\Omega_M$  if the concentration of particles within a distance  $h$  of the interface is above a given threshold  $c_{\max}$ . Conversely, we move the interface towards the compartment region  $\Omega_C$  if the concentration of molecules within the compartments on the boundary is less than  $c_{\max} - \delta c$ . In this way the maximum concentration expected in the molecular region is below  $c_{\max}$ . The difference between the two thresholds  $\delta c$  is necessary to prevent the spurious movement of the interface due to stochastic fluctuations in the molecule concentrations<sup>30</sup>. As we shall see, the reduction of  $\delta c$  to zero results in inaccuracies in the simulation that are due to rapid redistribution of molecules that occurs every time the interface  $I(t)$  moves into  $\Omega_M$ . We check for the upper and lower limit concentrations and move the interface every  $n_c$  timesteps of the simulation. Checking this condition at every time step ( $n_c = 1$ ) is unnecessary and can be computationally costly and therefore counterproductive to the purpose of using this multiscale method<sup>30</sup>.

After each check of the movement criteria, the interface  $I(t)$  can either move into the molecular region, or into the compartment region. If the former, then each molecule that is in the new compartment region (a perpendicular distance  $h$  from the old interface) is counted and placed inside the corresponding newly created compartment  $j_{\text{new}}$ . For each particle that is removed from the molecular-based simulation, the copy number in the new compartment  $A_{j_{\text{new}}}$  is incremented by one. If the interface moves into the compartment region then each com-

partment  $j$  which was previously adjacent to the interface and now in the new molecular region is removed and  $A_j$  new molecules are created within the space occupied by the old  $j$ -th compartment with randomly-generated, uniformly-distributed initial positions.

### III. RESULTS

Two model problems will be considered in this paper. In Section III A we demonstrate the impact of applying the ATRM to a simple morphogen gradient problem<sup>31,32</sup> with a known solution. This allows for an easy comparison between simulations using both static and moving interfaces. In this way, the error associated with the moving interface will be studied. In Section III B we use the ATRM to investigate Fisher waves in a molecular-based model.

#### A. Steady State Morphological Gradient

The simulation domain is a semi-infinite cuboid shown in Figure 3. The boundary at  $x = 0$  (coloured dark blue) is reflective and generates molecules with rate  $\lambda$ . There is no upper boundary in the  $x$  direction and the molecules are allowed to diffuse to  $x \rightarrow \infty$ . The compartment-based and molecular-based subdomains are labelled  $\Omega_C$  and  $\Omega_M$ , respectively. The interface between the subdomains is a plane perpendicular to the  $x$ -axis at  $x = I(t)$  and moves parallel to the  $x$ -axis with constant step size  $h$ . All boundaries in the  $y$  and  $z$  directions are periodic. One species  $A$  is simulated and moves with diffusion constant  $D$ . In addition to the production of molecules at  $x = 0$ , one unimolecular degradation reaction



is simulated. Thus, in the limit of high molecule copy numbers, the normal rate equations for this system give

$$\frac{da(x,t)}{dt} = D \frac{\partial^2 a(x,t)}{\partial x^2} - ka(x,t) + \lambda \delta(x)$$

where  $a(x,t)$ ,  $x \geq 0$ ,  $t \geq 0$ , denotes the concentration of  $A$  at any point  $(x,y,z) \in \Omega$ . This equation can be explicitly solved<sup>33</sup> to give

$$a(x,t) = \frac{\lambda}{2\beta D} \left[ e^{-\beta x} - \frac{e^{-\beta x}}{2} \operatorname{erfc} \left( \frac{2\beta Dt - x}{\sqrt{4Dt}} \right) - \frac{e^{\beta x}}{2} \operatorname{erfc} \left( \frac{2\beta Dt + x}{\sqrt{4Dt}} \right) \right] \quad (7)$$

where  $\beta = \sqrt{k/D}$ .

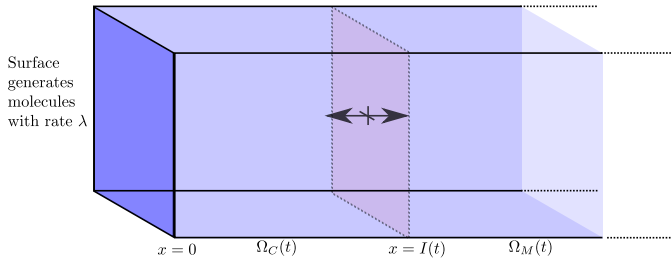


FIG. 3. The simulation domain  $\Omega = (0, \infty) \times (0, 1) \times (0, 1)$ . The moving interface is located at  $x = I(t)$ , and the compartment and molecular regions are  $\Omega_C = (0, I(t)) \times (0, 1) \times (0, 1)$  and  $\Omega_M = (I(t), \infty) \times (0, 1) \times (0, 1)$  respectively. Molecules are generated at the  $x = 0$  boundary (coloured dark blue) with rate  $\lambda$ . This boundary is also reflective. There is no lower boundary in the positive  $x$  direction. All other boundaries in the  $y$  and  $z$  directions are periodic.

Parameter	Value
$D$	1
$k$	10
$\lambda$	$10^6$
$\beta = \sqrt{k/D}$	$\sqrt{10}$
$h$	0.05
$\Delta t$	$10^{-4}$
$c_{max}$	$a_s(1/2) = 0.206 a_s(0)$
$\delta c$	$0.02 a_s(0)$
$n_c$	10

TABLE I. Table of simulation parameters for the morphological gradient simulation. The first three parameters are the parameters of the biological model ( $D$ ,  $k$  and  $\lambda$ ). Parameter  $h$  is the compartment size in  $\Omega_C$  and parameter  $\Delta t$  is the time step in  $\Omega_M$ . The last three parameters  $c_{max}$ ,  $\delta c$  and  $n_c$  are the parameters of the ATRM. The function  $a_s$  is given by (8).

### 1. Transient regime

The time-varying solution given in equation (7) has an initial transient period leading to a steady state solution

$$a_s(x) = \frac{\lambda}{2\beta D} e^{-\beta x} \quad (8)$$

as  $t \rightarrow \infty$ . This section examines the initial transient period, using the parameters given in Table I.

Figure 4 shows the results from a classical TRM simulation with a static interface  $I(t) \equiv 0.5$ , i.e. the bottom three parameters in Table I are not used. Four different timesteps (at  $t = 0.02, 0.06, 0.11$  and  $0.16$ ) were chosen from the transient period and the data from the molecular and compartment regions were plotted together in a one-dimensional concentration histogram along the  $x$ -axis. The bin size of the histogram was chosen to match the compartment size  $h$ . At all times shown, the concentration histogram data shows a good agreement with

the analytical solution  $a(x, t)$  in equation (7). Figure 5 shows similar results but from the ATRM simulation with a moving interface for parameters in Table I. The moving interface between the molecular and compartment regions correctly follows the maximum threshold set at  $c_{max} = 0.206 a_s(0)$ , and no noticeable differences can be seen between the static (TRM) and moving (ATRM) interface results.

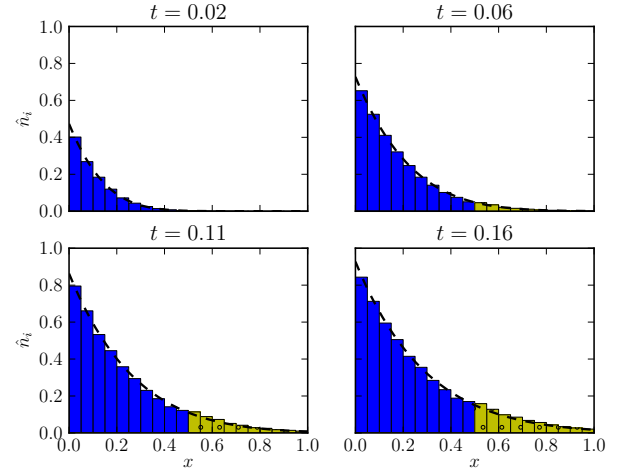


FIG. 4. Concentration histograms (along the  $x$ -axis) from the TRM simulation of morphogen gradient with  $I = 0.5$ . The concentration in each compartment  $\hat{n}_i$  has been scaled by the maximum expected concentration  $a_s(0)$ . Blue denotes the compartment-based region while yellow (with little circles) is used for the molecular-based region.

To measure the error, we count the number of molecules  $N(t)$  in the region  $(0, 0.5) \times (0, 1) \times (0, 1)$  and compare this to the number predicted by equation (7):

$$E(t) = \frac{N(t) - \int_{0.0}^{0.5} a(x, t) dx}{\int_0^\infty a(x, t) dx}. \quad (9)$$

For the static interface (TRM) case ( $I(t) \equiv 0.5$ ), this corresponds to comparing the total number of molecules in the compartment region with the expected amount. For the moving interface (ATRM) this is not the case, as the location of the interface varies with time. However, the movement threshold  $c_{max}$  is set so that the average steady state position of the interface is at  $x = 0.5$ , and therefore at steady state the position of the interface in the ATRM simulation will be consistent with the TRM case.

Figure 6 shows the error  $E(t)$  versus time for the static and moving boundary cases, along with a purely molecular-based simulation and a compartment-based simulation. The compartment-based simulation has its domain truncated at  $x = 2$  (with a reflective boundary condition). We expect only a very small number of molecules to reach  $x = 2$  so this truncation will introduce



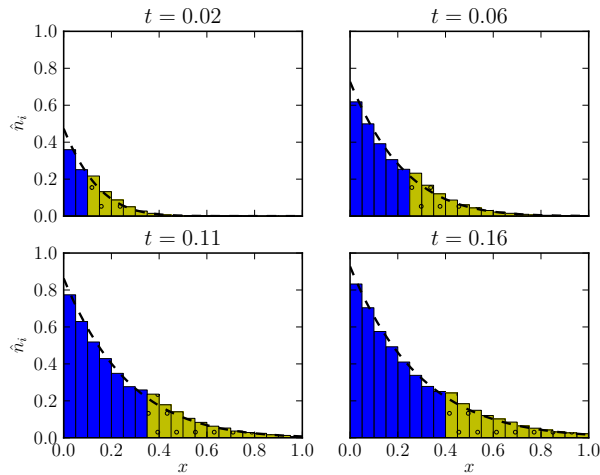


FIG. 5. Concentration histograms (along the  $x$ -axis) from the ATRM simulation of morphogen gradient with parameters given in Table I. The concentration in each compartment  $\hat{n}_i$  has been scaled by the maximum expected concentration  $a_s(0)$ . Blue denotes the compartment-based region while yellow (with little circles) is used for the molecular-based region.

negligible error. At very small times the error measure is dominated by the very low copy numbers in all simulations, but after  $t > 0.1$  it can be seen that both TRM and ATRM simulations lose molecules more rapidly from the  $x < 0.5$  region due to an overestimation of the diffusion across the interface. The absolute value of the error  $E(t)$  increases until  $t \approx 0.4$ , where it levels out at relatively low 2% of the total number of molecules. The effect of the moving boundary is small for these parameters, and the net effect of the moving boundary is to slightly decrease the diffusion of molecules across the interface. The next section explores further the moving interface error during the steady state, how this varies with the simulation parameters, and therefore, how it may be reduced.

## 2. Steady State Regime and Parameter Study

This section explores the effect of simulation parameters on the steady state error for static and moving interface simulations of the morphological gradient. Since we vary the compartment size  $h$  during these parameter sweeps, the concentration histograms are calculated using bins with a constant size of 0.05 along the  $x$ -axis (and with size 1 along the  $y$  and  $z$  axis). The contribution of each compartment  $i$  to bin  $j$  is scaled by the volume of  $i$  that overlaps with  $j$ . In order to calculate the steady state error,  $E(t)$  is averaged over 40 equally spaced times after steady state is reached at  $t = 5$  using

$$\hat{E} = \sum_{i=0}^{39} E(5 + i\tau) \quad (10)$$

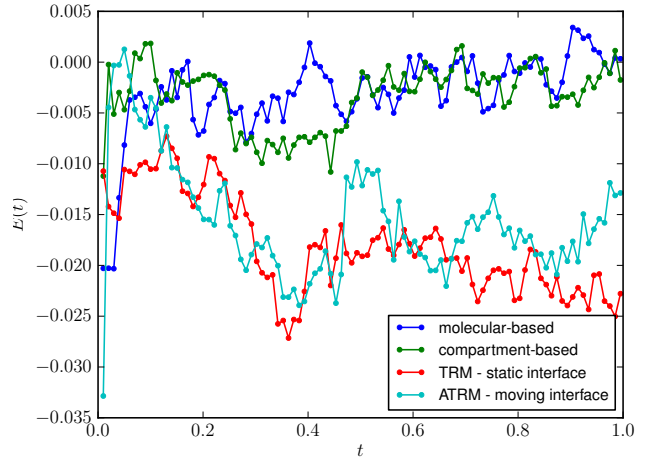


FIG. 6. Error  $E(t)$  given by (9) for four different simulation methods, pure molecular-based and compartment-based, along with the TRM and ATRM results.

where the spacing between each sample ( $\tau = 0.1$ ) is long enough so that there is no significant correlation between them.

Figure 7(a) shows the average steady state error  $\hat{E}$  versus compartment size  $h$  and average particle step size  $s = \sqrt{2D\Delta t}$ . The contour lines of constant  $\hat{E}$  generally follow a linear relationship between  $h$  and  $s$ , and the error is minimized near  $h = s$ . This is consistent with the convergence study described in<sup>34</sup>, which found that the TRM error for a static interface was minimized when  $h = \sqrt{\pi D\Delta t}$ . Figure 7(b) shows the same data in a scatter plot of  $\hat{E}$  versus  $h - \sqrt{\pi D\Delta t}$ , with each point is coloured by  $h$ . For a given  $h$  the error is linear with  $h - \sqrt{\pi D\Delta t}$  around the point  $h = \sqrt{\pi D\Delta t}$ , with a slope that varies with  $h$ . The change in slope with  $h$  is due to the  $\mathcal{O}(h^2)$  diffusion error in the compartment region, and is not seen in Flegg et al<sup>34</sup> since  $h$  is only refined near the interface. In our simulations  $h$  is refined over the entire compartment region and the  $\mathcal{O}(h^2)$  diffusion error becomes significant.

Figure 8 shows the steady state error  $\hat{E}$  for the ATRM simulation with moving interface. The most obvious change in  $\hat{E}$  with the moving interface is the shifting of the plots towards positive  $\hat{E}$ . That is, the flux of molecules across the interface towards the molecular region is (slightly) reduced. For intermediate and small values of  $h$  this reduction is small (1-2%), but for larger  $h$  the shifts become more pronounced due to much larger jumps that the interface makes. The scatter plot in Figure 8(right) also shows a strong non-linear reduction in  $\hat{E}$  for  $h \gg \sqrt{\pi D\Delta t}$ .

In summary, the effect of the moving interface on the error associated with the TRM is minimal, and generally in the region of 1-2% of the expected molecule concentration. This increases for larger  $h$  due to the larger step

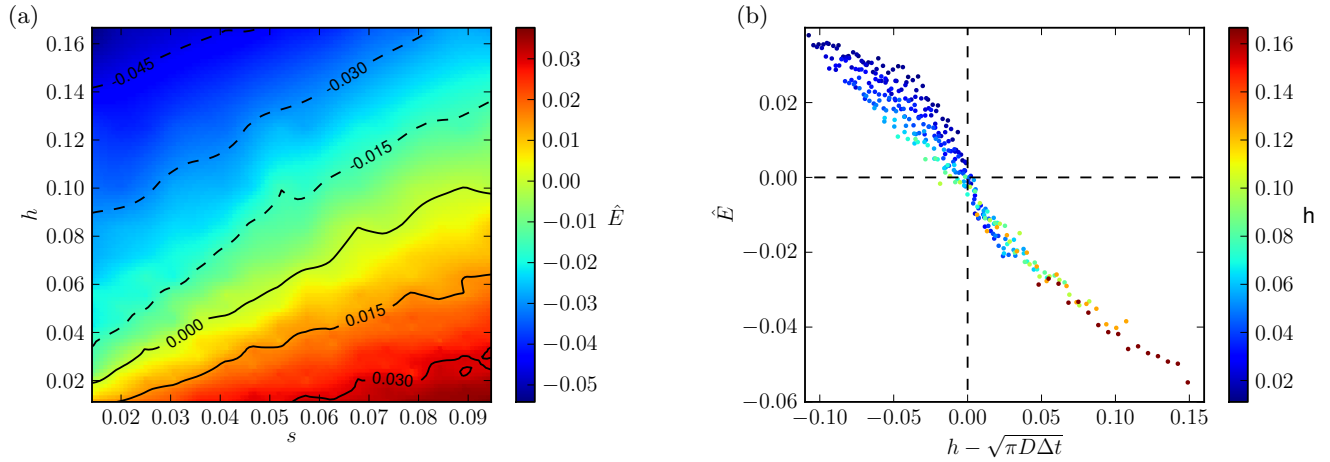


FIG. 7. (a) Colorplot of the TRM error  $\hat{E}$  given by equation (10) for steady state morphological gradient versus compartment size  $h$  and particle average step size  $s = \sqrt{2D\Delta t}$ ; (b) same data as a scatter plot of  $\hat{E}$  versus  $h - \sqrt{\pi D\Delta t}$ . Each point is coloured by  $h$ .

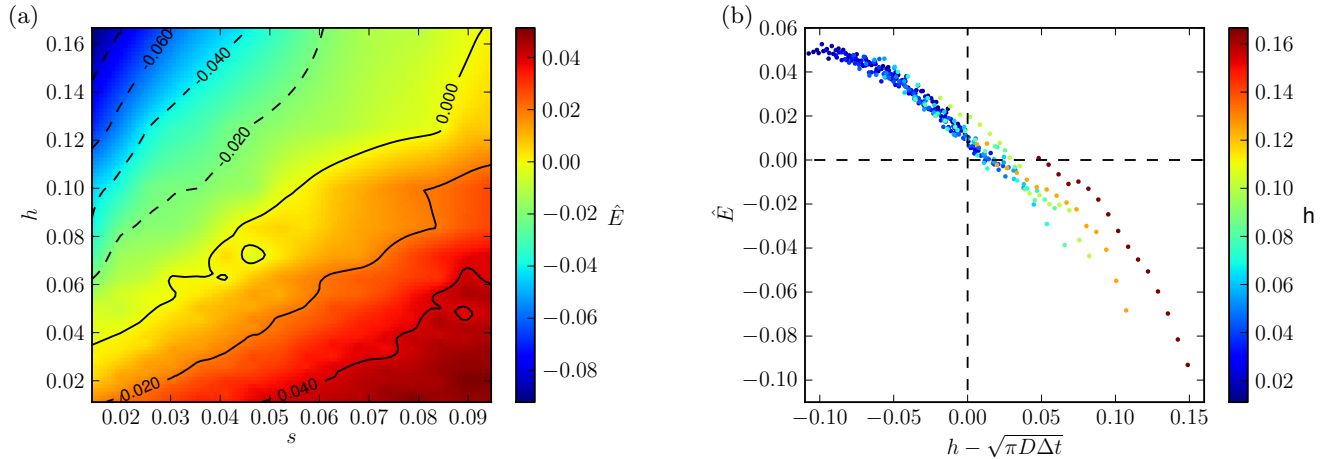


FIG. 8. (a) Colorplot of the ATRM error  $\hat{E}$  given by equation (10) for steady state morphological gradient versus compartment size  $h$  and particle average step size  $s = \sqrt{2D\Delta t}$ ; (b) same data as a scatter plot of  $\hat{E}$  versus  $h - \sqrt{\pi D\Delta t}$ . Each point is coloured by  $h$ .

size of the interface, but remains relatively small (less than 3%) unless  $h \gg \sqrt{\pi D\Delta t}$ , when it starts to diverge.

Figure 9 shows the same steady state error  $\hat{E}$  for the moving interface versus the ATRM parameters used to specify the movement criteria. These are  $\delta c$ , the separation between the upper and lower thresholds for movement, and  $n_c$ , the number of timesteps between checks of the movement criteria. For these simulations the resolution parameters are kept constant at  $h = 0.1$  and  $s = \sqrt{2D\Delta t} = 0.014$ . The results of this parameter sweep show that  $\delta c$  has the greatest effect on the error. The er-

ror decreases as  $\delta c$  is increased, and for these parameters is minimized for  $\delta c$  greater than 4% of the maximum steady state concentration  $a_s(0)$ . The error decreases more slowly for increasing  $n_c$ , and we also note that the increase in  $n_c$  also restricts the maximum speed of the moving interface. It is therefore clear that increasing  $\delta c$  is the optimal method to reduce the error associated with the moving interface.



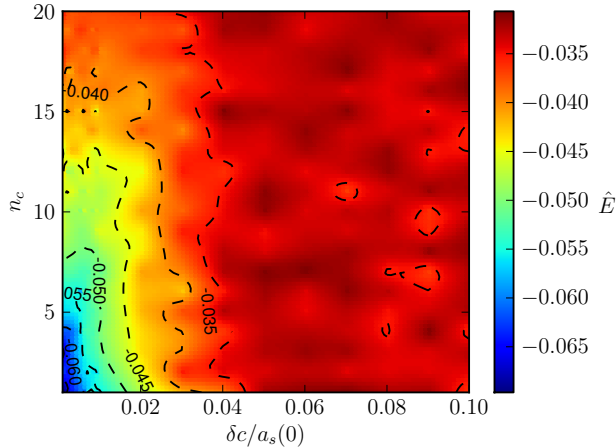


FIG. 9. Colorplot of the ATRM error  $\hat{E}$  given by equation (10) for steady state morphological gradient versus threshold separation  $\delta c$  and  $n_c$  of the ATRM.

## B. Fisher Wave

The Fisher equation<sup>11</sup> is the prototype model for the spread of a biological species and describes the diffusive spread of a species along with a logistic growth term

$$\frac{\partial u}{\partial t} = D\Delta u + k_1 u - k_2 u^2 \quad (11)$$

Given the phase space  $(u, \frac{\partial u}{\partial t})$ , the Fisher equation has unstable stationary point at  $(0,0)$  leading to a stable node at  $(k_1/k_2, 0)$ . It admits travelling wave solutions that transition from the unstable to the stable stationary point, which move with a wave speed  $c \geq 2$ . The wave will move with its minimum wave speed  $c = 2$  as long as the initial condition  $u(x, 0)$  is zero outside a finite domain<sup>1</sup>.

A single-species stochastic reaction-diffusion system matching the above PDE model can be constructed. Consider the evolution of a single species  $A$  which undergoes diffusion and a reversible reaction (2). Assuming a large number of molecules, the mean-field concentration of species  $A$  will approach equation (11). However, for low molecule copy numbers, stochastic effects can play an increasing role in the dynamics of the system. Numerous lattice-based models have shown that the stochastic fluctuations in the number of  $A$  molecules act to reduce the wave speed by a term  $c^*$  proportional to  $\log^{-2} N_0$ , where  $N_0$  is the average number of  $A$  molecules in each lattice site behind the wavefront<sup>12–14</sup>. This result, however, is not immediately applicable to molecular-based models, since  $N_0$  is inversely proportional to the volume of each lattice site and thus is determined by the lattice itself. While it would be useful to establish a similar scaling law for molecular-based methods, the computational requirements of such methods scale quickly with

increasing molecule numbers and it is therefore difficult to run the large simulations that are needed to approach the corresponding mean-field model.

The problem of running a stochastic travelling wave simulation with high molecule numbers is ideal for the ATRM. Setting the location of interface  $I(t)$  directly behind the wavefront means that the high concentration region behind the wave is modelled by the compartment-based method, while the wavefront itself and the low concentration region in front of the wave is modelled by the molecular-based method. Therefore the wave dynamics are captured entirely by the molecular-based method, while the total number of discrete molecules simulated is small and restricted only to those that can affect the wave propagation.

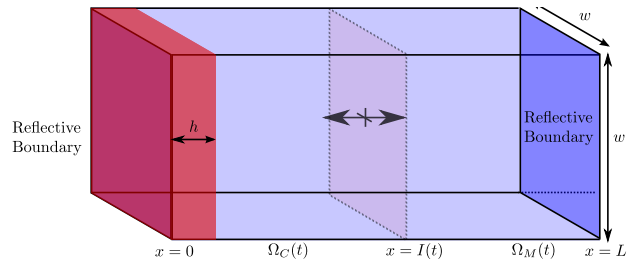


FIG. 10. Fisher wave simulation domain. Upper and lower  $x$ -axis boundaries are reflective. All other boundaries are periodic. The position of the (moving) interface between the molecular-based  $\Omega_M$  and compartment-based  $\Omega_C$  regions is  $x = I(t)$ . At  $t = 0$  the interface is located at  $x = I(0) = h$ , and the region  $x < h$  is filled with  $hw^2 k_1/k_2$  particles that are placed randomly within the region. The domain length is set to  $L$  and the height and depth of the domain are set to  $w$ .

Figure 10 shows the simulation domain  $\Omega = (0, L) \times (0, w) \times (0, w)$ . The initial conditions of the simulation are a random and homogeneous distribution of  $A$  molecules with concentration  $k_1/k_2$  over the volume defined by  $0 \leq x \leq h$  and  $0 \leq y, z \leq w$ . The domain in the  $y$  and  $z$  directions is periodic with length  $w$ , therefore the travelling wave will propagate as a one-dimensional wave in the positive  $x$  direction. The domain width is scaled by the expected concentration behind the wavefront  $w = \sqrt{800 k_1/k_2}$  in order to keep the total number of molecules constant with a varying reaction ratio  $k_1/k_2$ . The lower and upper  $x$  boundaries are both reflective. The interface between  $\Omega_M$  and  $\Omega_C$  is a plane with normal parallel to the  $x$ -axis and it moves with a step-size  $h$ . The parameters of the Fisher wave simulation are given in Table II. Three different stochastic simulations were run using (a) a purely compartment-based method, (b) a molecular-based method and (c) the ATRM method. A snapshot of each simulation taken at  $t = 40$  was shown in the introduction in Figure 1.

Our goal here is to ensure that the more efficient ATRM simulation matches the results obtained by the molecular-based method, and this is indeed the case. In Figure 1, both the ATRM (bottom panel) and the

Parameter	Value
$D$	1
$k_1$	1
$k_2$	1
$\rho$	0.5
$\alpha$	0.6
$P_{\Delta t}$	$3.7 \times 10^{-3}$
$h$	2.5
$\Delta t$	$10^{-3}$
$L$	100
$w$	28.3
$c_{max}$	$0.95 k_1/k_2 = 0.95$
$\delta c$	$0.55 k_1/k_2 = 0.55$
$n_c$	10

TABLE II. Table of parameters for the Fisher wave simulation, used in Figure 1. The first three parameters are the parameters of the biological model ( $D$ ,  $k_1$  and  $k_2$ ). Using (3), they were transformed to binding and unbinding radii  $\rho$  and  $\alpha\rho$ . Parameter  $h$  is the compartment size in  $\Omega_C$  and parameter  $\Delta t$  is the time step in  $\Omega_M$ . The last three parameters  $c_{max}$ ,  $\delta c$  and  $n_c$  are the parameters of the ATRM.

molecular-based (middle panel) simulation are very similar in terms of both the wavefront shape and propagation speed. However, clear differences can be seen in these wave speeds and those of the mean-field model and compartment-based simulation. These differences in wave speed and the effect of the parameters  $k_1/k_2$  and  $h$  are explored further on in this section.

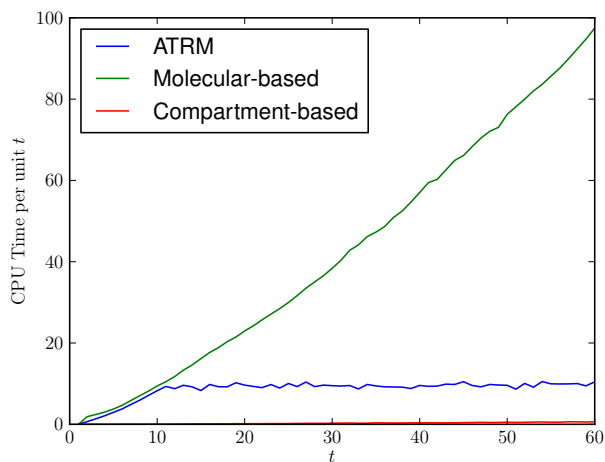


FIG. 11. Comparison of computational time for each of the simulation methods. The plots show the CPU time taken to simulate 1 second of each model as a function of time  $t$ .

To demonstrate the efficiency gained by using the ATRM method, Figure 11 shows a comparison of the

time taken to run each of the three different simulation methods. The plots show the CPU time taken to complete 1% of simulation time versus the total simulation percentage performed. The purely compartment-based method (red line) is clearly the fastest, and its plot can barely be seen at the bottom of Figure 11. The purely molecular-based simulation is the slowest. The ATRM simulation initially follows the molecular-based simulation, until the interface starts moving to follow the travelling wave at about  $t = 10$ . After this point there is a constant number of discrete molecules in the simulation (those in the wavefront itself) and therefore the simulation CPU time remains roughly constant.

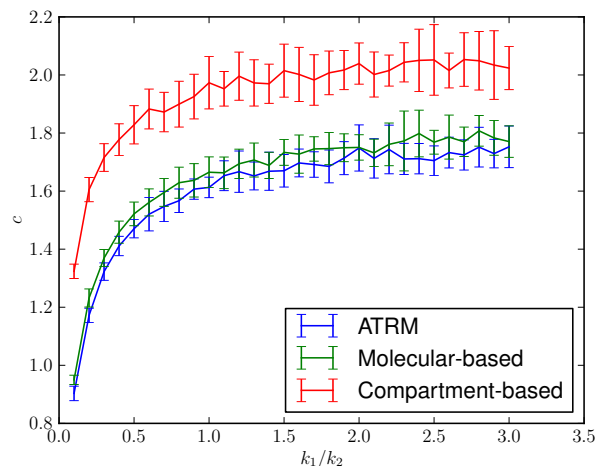


FIG. 12. Wave speed versus  $k_1/k_2$  for the three simulation methods. The wave speed is estimated using (12) from 20 different simulations, the average of these gives the solid line and the error bars show one standard deviation.

For a travelling wave simulation the important output measurement is normally the wave speed. Any stochastic simulation method must be able to accurately reproduce the speed of the wave and correctly capture any stochastic effects. Therefore we have measured the simulated wave speed versus the reaction ratio  $k_1/k_2$  and the compartment size  $h$ .

The reaction ratio  $k_1/k_2$  determines the saturation concentration of the wave (the concentration behind the wavefront) and therefore the number of molecules in the wavefront. Increasing this parameter increases the number of molecules in any given volume and therefore we would expect the wave speed to approach the mean-field wave speed  $c = 2$  as  $k_1/k_2$  increases for the compartment-based model. In the case of the molecular-based models, the mean-field PDE description is often justified under special circumstances (e.g. for systems with uniformly distributed reactants) and the convergence of travelling speeds to the mean-field model is not obvious.

Figure 12 shows the measured wave speed  $c$  versus  $k_1/k_2$  for the three different simulation methods. The

wave speed is measured as follows. Given the total number of molecules at a given time during the simulation  $N_{tot}(t)$ , we can obtain the estimate of the wave speed  $c$  as the appropriately rescaled rate of change of  $N_{tot}$  between two times  $t_1$  and  $t_2$ :

$$c = \frac{(N_{tot}(t_2) - N_{tot}(t_1))}{(t_2 - t_1)} \frac{k_2}{k_1 w^2}. \quad (12)$$

For each parameter value, we ran 20 Fisher wave simulations and calculate the wave speed using using  $t_1 = 10$  and  $t_2 = 30$ . The mean wave speed is plotted in Figure 12 as a solid line, while the error bars show one standard deviation.

The results show that the ATRM method with moving interface produces identical results to the purely molecular-based simulation for all values of  $k_1/k_2$ , within the range of stochastic fluctuations for the wave speed. As stated earlier, our goal is to match the results of the molecular-based method, which is achieved here. Note that the compartment-based method, while producing a similar scaling with  $k_1/k_2$ , gives a consistently higher wave speed than either of the other methods. This change in wave speed for the compartment-based method was found to vary with the compartment size  $h$ , and this is shown later on in Figure 13. However, while the ATRM simulation uses the compartment-based method for the domain behind the wavefront  $\Omega_C$ , the wave front is situated entirely in the molecular-based domain  $\Omega_M$  and thus the motion of the simulated wave is determined only by the molecular-based method. The diffusion error introduced by the ATRM interface is very small and has no effect on the simulation. Due to the position of the interface behind the wave front, the local concentration gradient is zero at the interface which results in a negligible ATRM diffusion error.

Figure 13 shows the measured wave speeds  $c$  versus the compartment size  $h$ . As previously stated, for the compartment-based method the wave speeds show a clear dependence on  $h$ . This result is not surprising, given that previous lattice-based simulations<sup>12–14</sup> showed a  $\log^{-2} N_0$  scaling for  $c$ , where  $N_0$  is the average number of molecules per lattice site and is therefore determined by the lattice spacing. In addition, the diffusion error in the compartment-based method is of order  $\mathcal{O}(h^2)$ , and for the Fisher wave this has the effect of increasing the wave speed enough that it becomes larger than the mean-field speed ( $c = 2$ ) for  $h \geq 3$ . However, neither of these effects apply to the molecular-based method, which does not have either a background lattice nor a set of compartments. The ATRM method, as desired, matches the molecular-based method perfectly and displays a constant wave speed versus  $h$ .

#### IV. DISCUSSION

We extended the TRM to consider a moving interface between the domains that can respond dynamically

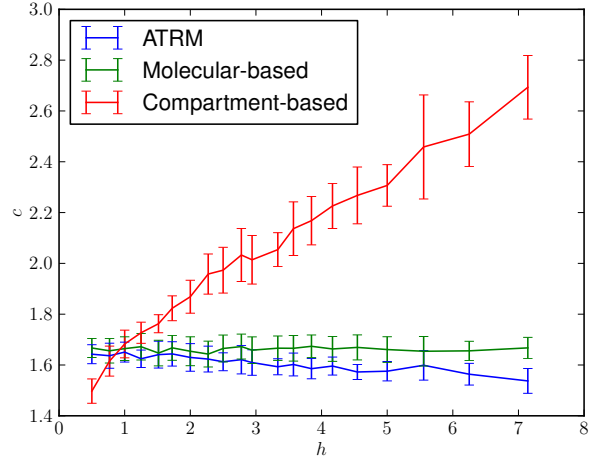


FIG. 13. Wave speed versus compartment size  $h$  for the three simulation methods. The wave speed is estimated using (12) from 20 different simulations, the average of these gives the solid line and the error bars show one standard deviation.

to the simulation variables (local concentration). This can be considered as an adaptive domain decomposition method, which motivates the addition of the word “Adaptive” to the TRM. The ATRM is a multiscale method aimed at coupling compartment and molecular-based stochastic reaction-diffusion simulations with a moving interface. In this paper, we applied it to two different problems, a morphological gradient problem with a steady-state solution and a Fisher travelling wave where the movement of the interface is determined by the wave motion.

The error associated with the moving interface for the steady-state morphological gradient case was investigated using parameter sweeps. It was found that effect of the moving boundary was minimal and that the additional error (over a static interface) was generally in the region of 1-2%. This error increases with  $h$ , the compartment size, and further increases for  $h$  much larger than  $\sqrt{\pi D \Delta t}$ , where  $D$  is the diffusion constant and  $\Delta t$  is the molecular-based timestep. The interface error was insensitive to the choice of  $n_c$  (minimum number of timesteps between interface movement), but it was found that  $\delta c$  (the separation between the upper and lower concentration thresholds) needed to be greater than 4% of the maximum molecular concentration for the error to be minimised.

The second test problem clearly showed the advantages of the ATRM method with a moving interface, applying the method to a travelling wave simulation using a single-species version of the classical Fisher equation. Here the wavefront was simulated by the molecular-based method while the compartment-based method was used for the high concentration region behind the front. The ATRM simulation showed a decrease in simulation time because

the simulation time is dominated by the molecules that are in the wave front itself, not those behind the wave front.

The wave speed  $c$  was measured for varying  $k_1/k_2$ , the ratio of the forward to backward reaction rates, and  $h$ , the compartment size. In all cases the measured wave speed was identical for both the TRM and the molecular-based simulations. All the methods showed an increase in wave speed with greater  $k_1/k_2$ . However, the wave speed for the compartment-based method showed a dependence on the  $h$ , which was not seen in either the ATRM or molecular-based results. Therefore, the ATRM method can be seen to match the molecular-based method, while at the same time being more computationally efficient. The error associated with the moving interface was negligible due to the location of the interface behind the wave front, where the concentration gradient is zero on average. The ATRM is therefore an ideal method to study the dynamics of a stochastic Fisher wave modelled using a molecular-based method, which would ordinarily be impractical due to the large number of molecules needed.

Another hybrid simulation approach would be to use a mean-field, deterministic, model for the simulation behind the wave front, which is then coupled to the molecular-based model for the wave front. This type of model has been used previously (but not applied to the Fisher wave) by Alexander et. al.<sup>35</sup>, Geyer et. al.<sup>36</sup> and Wagner and Flekkoy<sup>37</sup>. The disadvantage of coupling a mean-field model to a molecular-based model is that an overlap region is generally required in order to calculate the mass flux across the interface, and to accurately compute variances near the interface<sup>38</sup>. In contrast, using the combination of a compartment-based and molecular-based IBMs does not necessarily require an overlap region, and retains the stochastic nature of the model over the entire domain. We have also found the computational expense of the compartment-based model to be insignificant compared with the time spent on the molecular-based model (see Figure 11), so there is little motivation to use a mean-field model instead.

## ACKNOWLEDGEMENTS

This publication arises from research funded by the John Fell Oxford University Press (OUP) Research Fund. The research leading to these results has received funding from the European Research Council under the *European Community's* Seventh Framework Programme (*FP7/2007-2013*) / ERC grant agreement No. 239870. Radek Erban would also like to thank Brasenose College, University of Oxford, for a Nicholas Kurti Junior Fellowship; the Royal Society for a University Research Fellowship; and the Leverhulme Trust for a Philip Leverhulme Prize.

<sup>1</sup>J. Murray, *Mathematical Biology* (Springer Verlag, 2002)

- <sup>2</sup>A. Black and A. McKane, *Trends in Ecology and Evolution* **27**, 337 (2012)
- <sup>3</sup>D. Gillespie, A. Hellander, and L. Petzold, *Journal of Chemical Physics* **138**, 170901 (2013)
- <sup>4</sup>S. Andrews and D. Bray, *Physical Biology* **1**, 137 (2004)
- <sup>5</sup>J. Lipkova, K. Zygalkis, J. Chapman, and R. Erban, *SIAM Journal on Applied Mathematics* **71**, 714 (2011)
- <sup>6</sup>S. Engblom, L. Ferm, A. Hellander, and P. Lötstedt, *SIAM Journal on Scientific Computing* **31**, 1774 (2009)
- <sup>7</sup>R. Erban and S. J. Chapman, *Physical Biology* **6**, 046001 (2009)
- <sup>8</sup>W. van Gunsteren and H. Berendsen, *Molecular Physics* **45**, 637 (1982)
- <sup>9</sup>M. Smoluchowski, *Zeitschrift für physikalische Chemie* **92**, 129 (1917)
- <sup>10</sup>R. Erban, S. J. Chapman, and P. Maini, "A practical guide to stochastic simulations of reaction-diffusion processes," (2007), 35 pages, available as <http://arxiv.org/abs/0704.1908>
- <sup>11</sup>R. Fisher, *Annals of Eugenics* **7**, 355 (1937)
- <sup>12</sup>D. Panja, *Physics Reports* **393**, 87 (2004)
- <sup>13</sup>W. van Saarloos, *Physics Reports* **386**, 29 (2003)
- <sup>14</sup>É. Brunet and B. Derrida, *Journal of Statistical Physics* **103**, 269 (2001)
- <sup>15</sup>H. Breuer, W. Huber, and F. Petruccione, *Physica D: Nonlinear Phenomena* **73**, 259 (1994)
- <sup>16</sup>E. Moro, *Physical Review E* **69**, 060101 (2004)
- <sup>17</sup>M. Flegg, J. Chapman, and R. Erban, *Journal of the Royal Society Interface* **9**, 859 (2012)
- <sup>18</sup>M. Flegg, J. Chapman, L. Zheng, and R. Erban, "Analysis of the two-regime method on square meshes," (2013), submitted to *SIAM Journal on Scientific Computing*
- <sup>19</sup>R. Erban, M. Flegg, and G. Papoian, *Bulletin of Mathematical Biology* **to appear**, DOI: 10.1007/s11538 (2013)
- <sup>20</sup>S. Andrews, in *Bacterial Molecular Networks* (Springer, 2012) pp. 519–542
- <sup>21</sup>J. Stiles and T. Bartol, in *Computational Neuroscience: Realistic Modeling for Experimentalists*, edited by E. Schutter (CRC Press, 2001) pp. 87–127
- <sup>22</sup>R. Kerr, T. Bartol, B. Kaminsky, M. Dittrich, J. Chang, S. Baden, T. Sejnowski, and J. Stiles, *SIAM Journal on Scientific Computing* **30**, 3126 (2008)NoStop
- <sup>23</sup>B. Drawert, S. Engblom, and A. Hellander, *BMC Systems Biology* **6**, 76 (2012)
- <sup>24</sup>J. Elf and M. Ehrenberg, *Systems biology* **1**, 230 (2004)
- <sup>25</sup>D. Gillespie, *Journal of Physical Chemistry* **81**, 2340 (1977)
- <sup>26</sup>M. Gibson and J. Bruck, *Journal of Physical Chemistry A* **104**, 1876 (2000)
- <sup>27</sup>R. Erban and S. J. Chapman, *Physical Biology* **4**, 16 (2007)
- <sup>28</sup>J. Hattne, D. Fange, and J. Elf, *Bioinformatics* **21**, 2923 (2005)
- <sup>29</sup>M. Flegg, S. Rüdiger, and R. Erban, *Journal of Chemical Physics* **138**, 154103 (2013)
- <sup>30</sup>C.-P. Ho, *Multi-scale reaction diffusion simulations in biology*, M.Sc. Thesis, University of Oxford (2012)
- <sup>31</sup>F. Tostevin, P. ten Wolde, and M. Howard, *PLOS Computational Biology* **3**, 763 (2007)
- <sup>32</sup>M. Howard, *Trends in Cell Biology* **22**, 311 (2012)
- <sup>33</sup>S. Bergmann, O. Sandler, H. Sberro, S. Shnider, E. Schejter, B. Shilo, and N. Barkai, *PLoS Biology* **5**, e46 (2007)
- <sup>34</sup>M. Flegg, S. Hellander, and R. Erban, "Convergence of methods for coupling of microscopic and mesoscopic reaction-diffusion simulations," (2013), submitted to *Journal of Computational Physics*
- <sup>35</sup>F. Alexander, A. Garcia, and D. Tartakovsky, *Journal of Computational Physics* **182**, 47 (2002)
- <sup>36</sup>T. Geyer, C. Gorba, and V. Helms, *Journal of Chemical Physics* **120**, 4573 (2004)
- <sup>37</sup>G. Wagner and E. Flekkøy, *Philosophical Transactions of the Royal Society A: Mathematical, Physical & Engineering Sciences* **362**, 1655 (2004)
- <sup>38</sup>B. Franz, M. Flegg, J. Chapman, and R. Erban, *SIAM Journal on Applied Mathematics* **73**, 1224 (2013)